Journal of Catalysis 270 (2010) 196–205

Contents lists available at ScienceDirect

Journal of Catalysis

journal homepage: www.elsevier.com/locate/jcat

Pinacol-type rearrangement catalyzed by Zr-incorporated SBA-15

Shih-Yuan Chen [a], Jyh-Fu Lee [b], Soofin Cheng [a,*]

[a] Department of Chemistry, National Taiwan University, Taipei 106, Taiwan
[b] Research Division, National Synchrotron Radiation Research Center, Hsinchu 300, Taiwan

ARTICLE INFO

Article history:
Received 15 November 2009
Revised 14 December 2009
Accepted 25 December 2009
Available online 22 January 2010

Keywords:
SBA-15
Zirconium
Mesoporous materials
One-pot synthesis
Pinacol rearrangement
Pinanediol

ABSTRACT

Highly ordered zirconium-incorporated SBA-15 materials, designated as Zr–SBA-15, with Zr/Si ratios up to 10.8 mol% were one-pot synthesized in a self-generated acidic environment. Zr was incorporated into the SBA-15 framework as isolated Zr species, and it also formed superficial zirconia clusters with two or more Zr centers on the pore walls when the Zr/Si ratio was higher than 3 mol%. The acid amounts of Zr–SBA-15 materials increased linearly with Zr loading, but the acidities were lower than those of commercially available HY and ZSM-5 zeolites. However, when used as the catalysts in liquid phase pinacol-type rearrangement, one-pot synthesized Zr–SBA-15 materials, especially those with superficial zirconia clusters, were the most efficient catalysts. The pinacolone yield of 2.7 g/g catal h and selectivity of 81% were achieved in 1 h over Zr–SBA-15 with a Zr/Si ratio of 10.8 mol%. Moreover, Zr–SBA-15 was also efficient in catalyzing the rearrangement of bulky 2,3-pinanediol to yield camphor as the major product through hydrogen migration.

1. Introduction

Mesoporous silica materials possessing high surface areas and ordered mesoporous structures show potential applications in separation [1], enzyme immobilization [2], catalysis [3,4], nanocasting [5,6] and electro-optical devices [7–9]. Among the mesoporous materials, SBA-15 with tunable pores in 4–10 nm arranged in 2D-hexagonal *p6mm* structure has received great attention in the past decade because of its relatively large pore size and high hydrothermal stability in comparison with other mesoporous silica materials, such as MCM-41, its analog in M41S family [10,11]. Since pure siliceous mesoporous materials are chemically inert and have poor catalytic activities, great efforts have been devoted to prepare mesoporous silica materials modified with various functionalities such as organic groups, transition metals and metal complexes through surface grafting or co-condensation [3,4,12–22]. Co-condensation method is favored to surface grafting due to better control in the loading and distribution of the functional groups. Many metals and metal oxide species, including Zr [14,15], Al [16], Ti [17,18], Fe [19], Sn [20], Au [21] and Pt [22], have been incorporated into SBA-15 by co-condensation. However, the pore ordering is difficult to retain when large amounts of the hetero-elements were introduced into the silica framework, due to the disturbance of the self-assembly of surfactant micelles and silicate by the precursors of hetero-elements [15,17,18]. Moreover, the strong acidic environment (usually ca. 2 M HCl) encountered in the synthesis of SBA-15 also impedes the precipitation of metal oxides. Our group previously developed an environmentally friendly process for synthesizing metal-incorporated SBA-15 of well-ordered mesoporous structure with the metal loading up to 10 mol%, without using mineral acids and with the aid of salts [4,14,20].

Pinacol rearrangement is a valuable process for preparing aldehydes or ketones through the skeletal rearrangement of 1,2-diols and elimination of water. The reaction is usually carried out in the presence of at least an equimolar amount of strong mineral acids, such as H_2SO_4 or $HClO_4$ [23–27]. Our previous studies showed that pinacol rearrangement could be catalyzed by metal-incorporated molecular sieves at relatively mild temperatures [26]. In the present work, the Zr-incorporated SBA-15 materials were examined as the catalysts in the pinacol-type rearrangement. The Zr–SBA-15 materials with Zr/Si ratio higher than 0.05 were found to be efficient catalysts, and the possible active sites in Zr–SBA-15 were proposed.

2. Experimental

2.1. One-pot synthesized Zr–SBA-15

One-pot synthesized Zr–SBA-15 materials with various Zr loadings were prepared by the procedures described in our previous paper [14]. Typically, 1 g of amphiphilic P123 triblock copolymer (Aldrich, M_n = 5800), 0.59 g of sodium chloride (NaCl, Acros) and various amounts of zirconyl chloride octahydrate ($ZrOCl_2{\cdot}8H_2O$, Acros) were dissolved in 40 g of de-ionized water at 35 °C, followed

* Corresponding author. Fax: +886 2 2363 6359.
E-mail address: chem1031@ntu.edu.tw (S. Cheng).

0021-9517/$ - see front matter © 2009 Elsevier Inc. All rights reserved.
doi:10.1016/j.jcat.2009.12.020

by adding 2.1 g of tetraethyl orthosilicate (TEOS, Acros). The compositions of the reactants were 0.017 P123:1 TEOS:0.01–0.1 $ZrOCl_2{\cdot}8H_2O$:221 H_2O:1 NaCl. The mixture was stirred in a sealed bottle at 35 °C for 24 h, and then heated under static condition at 90 °C for another 24 h. The solid products were collected by filtration, washed with large amount of de-ionized water and dried at 50 °C overnight. The template was removed by calcining the solids at 500 °C for 12 h with a heating rate of 1 °C/min. The calcined samples were designated as xZr–SBA-15, where "x" is the Zr/Si molar ratio in the synthesis gel.

2.2. References materials

Zr-impregnated SBA-15 materials with Zr/Si ratios of 0.03 and 0.1 (shortly termed ImZr–SBA-15) were prepared by slowly adding 5 mL of 0.1 M or 0.33 M $ZrOCl_2$ solution into 1 g of calcined siliceous SBA-15 (shortly termed Si–SBA-15), which was prepared according to the procedures reported by Zhao et al. [10]. After stirring for 10 min, the solvent was removed by rotary evaporation. The resultant materials were dried at 50 °C overnight and then calcined at 500 °C for 12 h. A ZSM-5 sample with SiO_2/Al_2O_3 ratio of 230, Na_2O content of 0.045 wt%, and surface area of 402 m^2/g was purchased from Advchem Lab. Inc., Taiwan. A HY-zeolite sample with SiO_2/Al_2O_3 ratio of 5.31, Na_2O content of 1.1 wt%, and surface area of 692 m^2/g was supplied as one of the Japanese Reference Catalysts (JRC-Z-HY5.3) from Catalysts and Chemicals Ind. Co., Ltd. (CCI), Japan.

2.3. Characterization

Powder X-ray diffraction (XRD) patterns were recorded in the 2θ ranges of 0.5–5° and 10–80° using a Philips X'pert Pro diffractometer with Cu Kα radiation (λ = 1.5418 Å) operating at 40 mA and 45 kV. The textural properties of the samples were analyzed by nitrogen physisorption at liquid nitrogen temperature (−196 °C) with a Micrometrics Tristar 3000 instrument. Prior to the measurements, the sample was out-gassed at 200 °C for 6–8 h under vacuum (10^{-3} Torr). The specific surface areas were determined using Brunauer–Emmett–Teller (BET) method in the P/P_0 range around 0.05–0.3. Pore size distribution (PSD) curve was calculated by Barrett–Joyner–Halenda (BJH) method using the desorption branch of the isotherm. Pore sizes were obtained from the peak positions of the distribution curves. The elemental contents in bulk were determined with an inductive-coupled plasma-atomic emission spectroscopy (ELAN 5000 ICP-AES instrument). Typically, the samples (ca. 20 mg) were dissolved in a 50 mL of mixed HF–HCl solution, and the solution was diluted 50 times prior to the measurement. The thermogravimetric (TG) analysis was carried out on a DuPont 951 TG analyzer under 50 mL/min air flow. Temperature-programmed desorption of ammonia (NH_3-TPD) was performed by a Micrometrics Autochem 2910 system equipped with a Thermo-ONIX mass selective detector. Prior to the measurements, the samples (ca. 200 mg) were pre-treated at 500 °C for 1 h under He atmosphere to eliminate physically adsorbed water, and then cooled to 100 °C for adsorption of NH_3 for another 1 h. The NH_3-TPD profiles were measured over the temperature range from 100 and 800 °C using He as a carrier gas. The Zr *K*-edge X-ray absorption spectra were taken at beam line 01C at National Synchrotron Radiation Research Center (NSRRC) at Hsinchu, Taiwan, under a standard operating condition of 1.5 GeV and 300 mA. The photon energies were calibrated using the *K*-edges of Zr foils at 17.998 keV. The scanning electron microscopy (SEM) photographs were taken using a Hitachi S-800 Field Emission Scanning Electron Microscope operating with a 20 keV field emission gun. Sample in the form of a fine powder was stuck on the copper holder and then coated with a thin layer of gold–palladium alloy by vacuum sputtering method. The energy-dispersed X-ray spectra (EDS) were taken with a Hitachi S-2400 Scanning Electron Microscope. Sample preparation was similar to that of SEM experiment except the sample was stuck on a carbon sample holder without over coating the metal layer. Each datum was the average of more than 20 analysis spots. The transmission electron microscope (TEM) experiments were performed on a Hitachi H-7100 Transmission Electron Microscope operating with a 75 keV electron gun. The powder sample was mixed with epoxy resin and solidified at 70 °C for 24 h. The immobilized sample was sliced into films in ca. 90 nm thickness with a RMC MTXL Cryo-ultramicrotome for TEM studies. The diffuse-reflectance (DR) UV–Vis spectroscopy was measured by a Hitachi U-3310 spectrophotometer equipped with an integrating sphere detector. Barium sulfate was used as a reference material.

2.4. Pinacol-type rearrangement

The liquid phase pinacol-type rearrangement was carried out in a 3-necked flask connected with a water cooling condenser and a thermometer. Pinacol-type reactant of 0.1 g dissolved in 5 g of toluene was refluxed at 110 °C before introducing the catalyst, which was pre-dried at 200 °C overnight. The reactant to catalyst weight ratio was kept at 5. The products were separated using a HP 6890 gas chromatograph (GC) and qualitatively identified with a HP 5973 mass selective detector. The quantitative analyses of the products were carried out using a Shimadzu GC-14B GC equipped with a FID detector, and 1,3,5-trimethylbenzene was used as an internal standard.

3. Results and discussion

3.1. Characterization of one-pot synthesized Zr–SBA-15

3.1.1. XRD

The XRD patterns of calcined Zr–SBA-15 materials with various Zr/Si ratios are shown in Fig. 1. In the small-angle region,

Table 1
Elemental analysis and textural properties of calcined Zr–SBA-15 with various Zr loadings.

Zr/Si (gel)	Zr/Si (solid)		pH (gel)	a_0 (nm)	S_{BET} (m^2/g)	V_{Total} (cm^3/g)	Φ_P[a] (nm)	PSD (nm)	W_t[b] (nm)	Yield[c] (%)
	ICP-AES	EDS								
0.010	0.017	0.018	2.4	12	840	1.0	7.1	1.2	5	~100
0.030	0.029	0.047	1.9	12	800	0.90	7.1	1.3	5	~100
0.040	0.044	0.067	1.8	12	800	1.0	7.1	1.3	5	~100
0.050	0.059	0.078	1.7	12	780	0.90	6.6	1.3	5	~100
0.10	0.11	0.15	1.5	12	720	0.90	6.1	1.5	6	~100

[a] Pore diameter measured at the maximum of the BJH PSD.
[b] $W_t = a_0 - \Phi_P$.
[c] The molar yields of silica materials based on the residues of TG analyses.

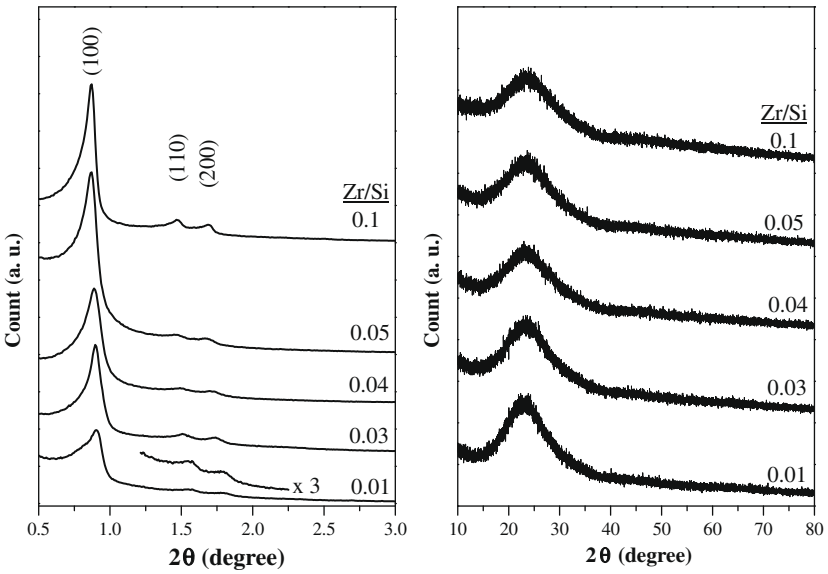

Fig. 1. Small and wide-angle XRD patterns of calcined Zr–SBA-15 materials with various Zr/Si ratios.

all materials show strong (1 0 0), (1 1 0) and (2 0 0) diffraction peaks of 2D-hexagonal *p*6*mm* structure, indicating that the materials possess well-ordered pore arrangement [10,11]. Moreover, the pore ordering is not significantly affected by increasing the Zr loadings. In the wide-angle region, calcined Zr–SBA-15 materials showed a broad diffraction peak at 2θ around 15–35°, which is corresponding to amorphous silica walls of mesoporous materials. In addition, no crystalline zirconium oxides were detected, implying that the Zr species were homogeneously dispersed in SBA-15.

3.1.2. Elemental analysis and product yields

The chemical properties of calcined Zr–SBA-15 materials are tabulated in Table 1. The pH values of the synthesis solutions were varied in 1.51–2.40, and the acidities were proportional to the amounts of Zr precursors added. The yields of Zr–SBA-15 with Zr/Si molar ratios varied in 0.01–0.1 were all close to 100%, indicating that the acidities generated by the zirconium precursor, $ZrOCl_2$, are enough to catalyze the hydrolysis and condensation of TEOS. Both ICP-AES and EDS techniques were applied to analyze the elemental compositions. The Zr/Si molar ratios in bulk measured by ICP-AES were very close to those in the synthesis gels, implying that the co-precipitation of zirconium and silicate species was almost complete. On the other hand, the Zr/Si molar ratios measured by EDS technique were significantly higher than those by ICP-AES when the Zr/Si ratios were larger than 0.03. Since EDS is a surface-sensitive technique, zirconium may be concentrated on the superficial areas of the SBA-15 walls when the Zr/Si ratios are larger than 0.03.

The addition of NaCl seems to facilitate the self-assembly of P123 micelles and silicate, and lead to highly ordered mesoporous structures. However, the sodium and chloride ions were not incorporated into the SBA-15 framework based on the ICP-AES and EDS analyses. In addition, the Zr loadings in the SBA-15 materials prepared by the present method do not change significantly with or without NaCl in the synthesis solution. Previous studies have shown that the critical micelle concentration of P123 decreases in the presence of salts, such as NaCl, KCl and so on [28–33]. This is the so-called salting-out effect. Moreover, it is also noticed that the silica condensation is more complete when preparing the mesoporous silica materials with NaCl [32,33]. It is attributed to that the interaction between P123 micelles and silicate is enhanced when the ionic strength of the synthesis solution is increased.

3.1.3. Electron microscopy

The SEM and TEM photographs of calcined Zr–SBA-15 materials with various Zr/Si ratios are shown in Fig. 2. The material is composed of interconnected rod-like particles in fiber-like morphology of ca. 500 nm in width and 10–55 μm in length. TEM photographs of the cross-sections of the particles show well-ordered 2D-hexagonal *p*6*mm* pore arrangement. The mesochannels are aligned along the long axis of the fibers. No ZrO_2 particles were observed, indicating that Zr species are homogenously incorporated in the SBA-15 framework. It is also noticed that all the Zr–SBA-15 materials with different Zr/Si ratios have similar morphology and mesostructure.

3.1.4. Nitrogen adsorption–desorption isotherms

The nitrogen sorption isotherms and PSD curves of calcined Zr–SBA-15 are shown in Fig. 3. All of them possessed type IV isotherms with H_1 hysteresis loops analogous to that of conventional Si–SBA-15 [10]. The parallel hysteresis loops at P/P_0 around 0.6–0.8 are the characteristics of highly ordered large mesopores with narrow PSD. The textural properties of Zr–SBA-15 materials are also summarized in Table 1. The unit cell parameters (a_0) and PSDs of Zr–SBA-15 are independent of the Zr loadings. On the other hand, the surface area (S_{BET}), pore volume (V_{Total}) and pore diameter (Φ_P) decreased gradually with the Zr loading in SBA-15 materials, while the trend for wall thickness (W_t) was in reverse. These results are one of the indications that Zr species are incorporated in the silica framework without significantly blocking of the mesopores.

3.1.5. TG analysis

The TG analysis has been found to be a useful tool for probing the interaction between the surfactant and inorganic framework [10,14,20]. Fig. 4 shows the TG and differential thermogravimetric (DTG) profiles of as-made Zr–SBA-15 materials in comparison with those of conventional Si–SBA-15. The P123 copolymer in conventional Si–SBA-15 decomposed in a single step at 180–250 °C with a weight loss around 53 wt%, similar to that of previous report [10]. The amounts of P123 copolymer in the Zr–SBA-15 materials were within 48–57 wt% and slightly varied with the Zr/Si ratios. Two signals were observed in the DTG profiles of Zr–SBA-15

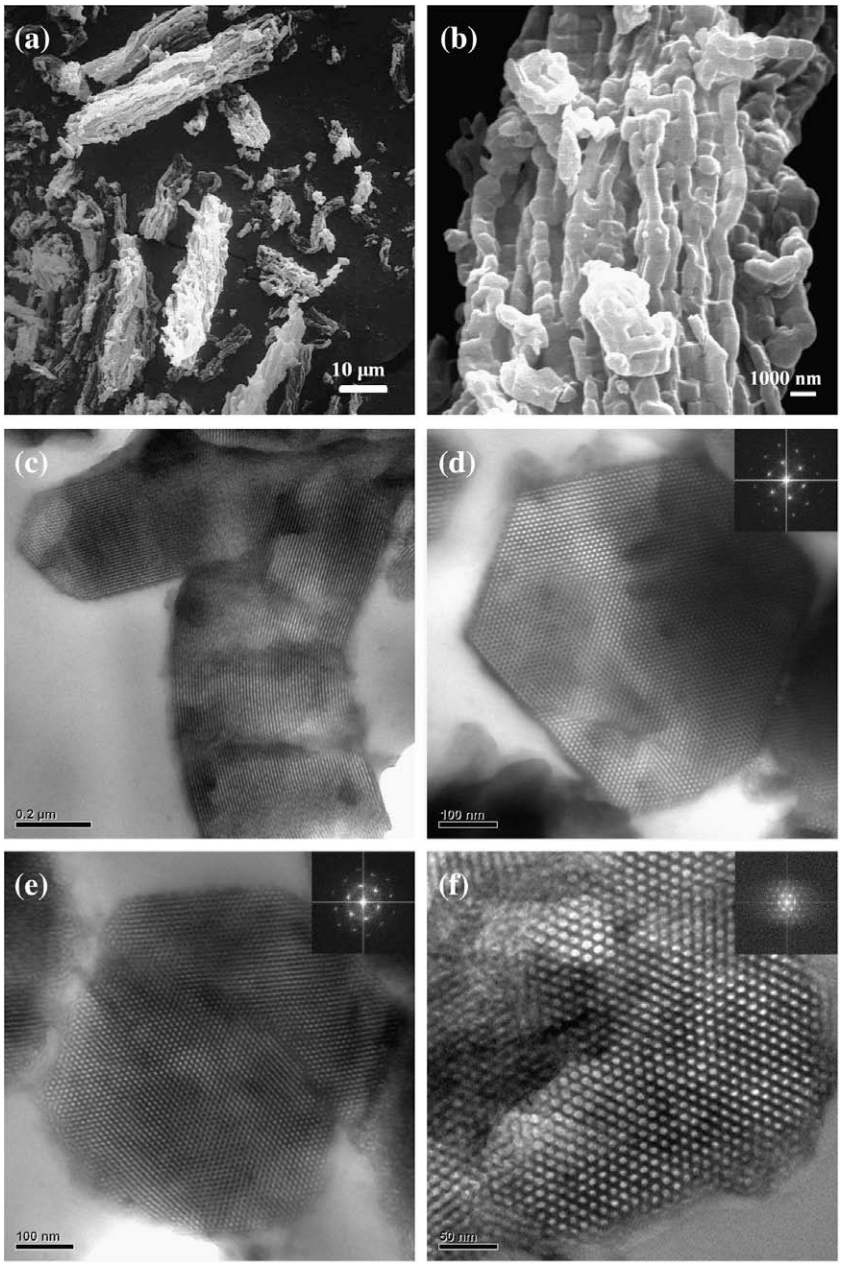

Fig. 2. SEM and TEM photographs of calcined Zr–SBA-15 with Zr/Si ratios of (c and d) 0.01, (a, b and e) 0.05 and (f) 0.1.

materials, implying that at least two different interactions between P123 copolymer and inorganic pore wall are present. One DTG signal with the maximum at ca. 190 °C was found in Si–SBA-15 and Zr–SBA-15 materials with Zr/Si ratios lower than 0.05. Moreover, its intensity decreased with the increase in Zr/Si ratio. This signal is attributed to the decomposition of P123 copolymer interacting with the silica pore wall [10,14,20]. For the samples with Zr/Si ratio larger than 0.03, the other DTG signal was gradually observed at higher temperature region. This peak shifted from 205 to 300 °C as the Zr/Si ratio increased from 0.01 to 0.05, and then stayed at ca. 300 °C even the Zr/Si ratio was further increased to 0.1. These results imply that a stronger interaction force between P123 copolymer and inorganic pore wall is present when the Zr/Si ratios are larger than 0.03. Since elemental analyses show that Zr is more concentrated on the wall surfaces with these loadings, the increase in decomposition temperature of P123 in Zr–SBA-15 materials is probably attributed to the stronger interaction between P123 copolymer and the superficial Zr species on the pore walls. The diminishing of DTG peak at 190 °C and the growth of the higher temperature peak indicate that the silica surfaces of pore walls are gradually covered up by the Zr species. When the Zr/Si ratio is increased to 0.07, the incorporated Zr seems to form a thin layer of superficial Zr species, and silica is no longer exposed to interact with P123.

3.1.6. DR UV–Vis spectroscopy

UV–Vis spectroscopy was used to study the dispersion and chemical environment of hetero-elements incorporated in silica materials [20,34,35]. The DR UV–Vis spectra of calcined Zr–SBA-15 materials with various Zr/Si ratios were compared with those of ImZr–SBA-15, $ZrOCl_2{\cdot}8H_2O$ and bulk ZrO_2 (Fig. 5). $ZrOCl_2{\cdot}8H_2O$ is an hydroxide-containing cluster consisting of the cation $[Zr_4(OH)_8(H_2O)_{16}]^{8+}$. This Zr_4 tetramer features four pairs of hydroxide bridging ligands linking four $Zr(H_2O)_4^{4+}$ centers [36].

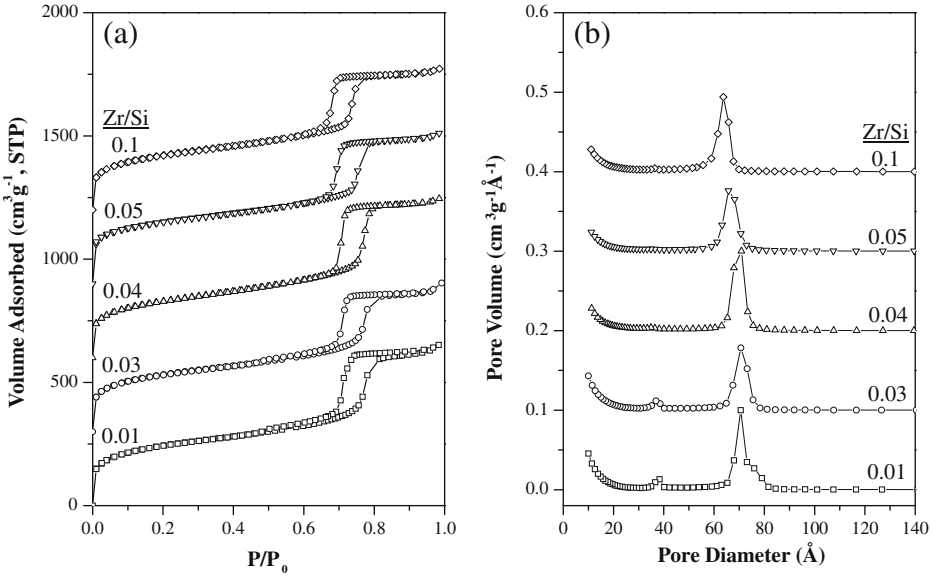

Fig. 3. (a) N_2 adsorption–desorption isotherms and (b) BJH PSDs of calcined Zr–SBA-15 materials with various Zr/Si ratios.

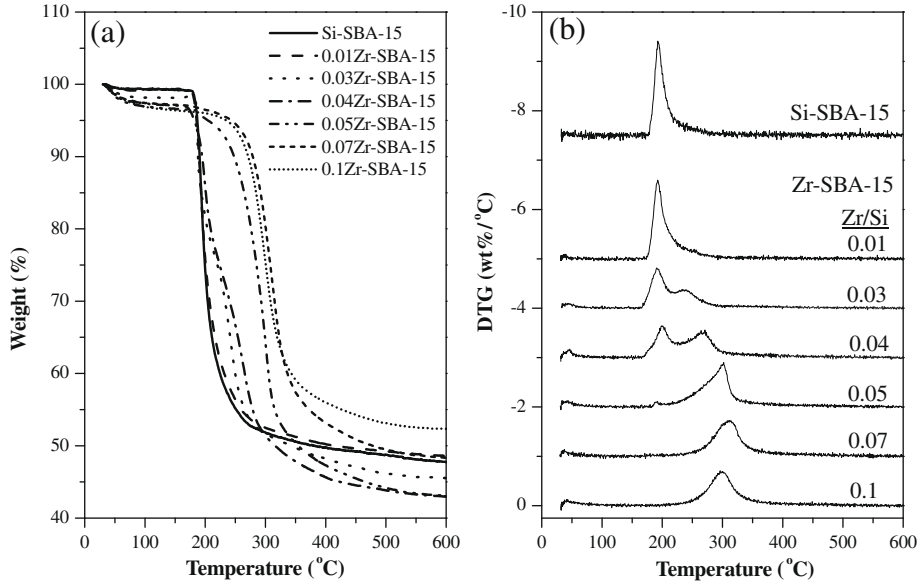

Fig. 4. (a) TG and (b) DTG profiles of as-made Zr–SBA-15 materials in comparison with those of Si–SBA-15.

The absorption at ca. 200 nm is due to the O → Zr(IV) LMCT (ligand to metal charge transfer) transition at the 8-coordinated Zr in distorted square antiprismatic structure. ZrO_2 of mixed tetragonal (8-coordinated Zr) and monoclinic (7-coordinated Zr) phases has a broad absorption band in 195–245 nm, which is composed of three peaks centered at 195, 211 and 227 nm, and a very weak band covering 250–360 nm. The 195–245 nm band is attributed to the overlap of the O → Zr(IV) LMCT transition, and the electron transition from the valance band to the conduction band of ZrO_2 crystallites [34]. The band gap determined from the spectrum is 4.80 eV, which is similar to the literature report [34]. The weak broad band covering 250–360 nm may be a consequence of transitions from extrinsic states involving surface defects or impurities [35]. ImZr–SBA-15 materials have relatively broad bands covering 195–235 nm with a maximum at 200–209 nm. It is attributed to the overlap of the O → Zr(IV) LMCT and the band gap transitions. The energy gaps of 5.1–5.2 eV are blue shifted in comparison with that of bulk ZrO_2 and that is due to quantum size effect since Zr probably forms small ZrO_2 crystallites in ImZr–SBA-15.

The UV–Vis spectra of Zr–SBA-15 materials did not resemble those of bulk ZrO_2, $ZrOCl_2{\cdot}8H_2O$ or ImZr–SBA-15, inferring that Zr probably forms different species. A narrow band at ca. 194 nm was observed for the low Zr loading samples, which is attributed to O → Zr(IV) LMCT. With the increase in Zr content, another peak appeared at around 205 nm. When the Zr/Si ratio was raised to 0.1, the 194 nm LMCT band was almost gone and the 205 nm peak was predominant. In combination with the results of XRD, TG and UV–Vis studies, Zr in the one-pot synthesized Zr–SBA-15 samples with Zr/Si ratios varied in 0.01–0.05 should be mainly isolated Zr species well dispersed in the silica framework. With the increase in Zr loading, Zr may migrate out of the silica framework and form extra-framework ZrO_2 clusters on the superficial areas of pore walls. Therefore, the 205 nm peak is due to the band gap transition in small ZrO_2 clusters. The relative blue shift of the band gap

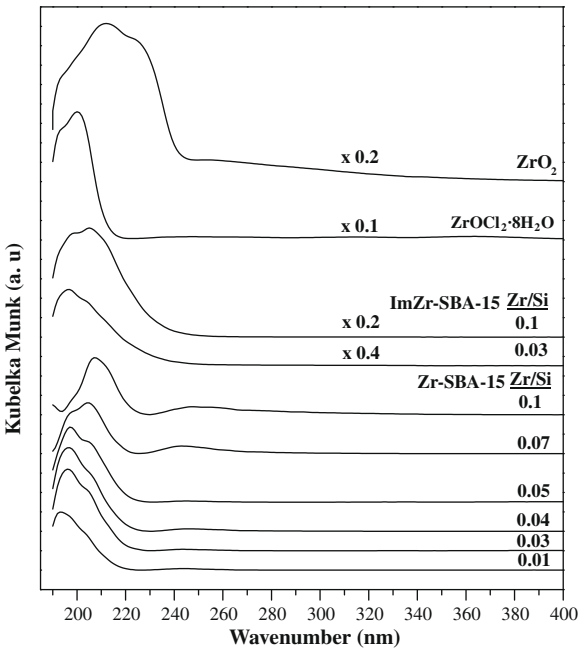

Fig. 5. DR UV–Vis spectra of commercial ZrO_2 and $ZrOCl_2{\cdot}8H_2O$, ImZr–SBA-15 and calcined Zr–SBA-15 materials with various Zr/Si ratios.

transition in comparison with that of ImZr–SBA-15 indicates that the sizes of the extra-framework ZrO_2 clusters are much smaller than the ZrO_2 crystallites prepared by impregnation method.

3.1.7. Zr K-edge X-ray absorption spectroscopy

X-ray absorption spectroscopy is a powerful technique to study the local structures of targeted elements, even in the amorphous solids and semi-crystalline nanoparticles [14,37–39]. The Zr *K*-edge X-ray absorption spectra were Fourier transformed into *r* space, and the $\chi(k) * k^3$ weighted spectra of as-made and calcined Zr–SBA-15 materials were compared with those of a diluted $ZrOCl_2$ solution (7.6 mM), bulk ZrO_2 and ImZr–SBA-15 samples with Zr loadings of 3 and 10 mol% (Fig. 6). For the $ZrOCl_2$ solution, two scattering features were observed at 1.68 and 3.22 Å (uncorrected), which were assigned to the eight nearest oxygen atoms and three neighboring Zr atoms in the $[Zr_4(OH)_8(H_2O)_{16}]^{8+}$ ion. For bulk ZrO_2, three strong scattering features were seen at 1.61, 3.06 and 3.45 Å (uncorrected), attributed to the nearest oxygen and neighboring Zr atoms, respectively, and some weak scattering features of further shells were also seen above 4 Å. The spectrum is consistent with that of crystalline ZrO_2 in monoclinic structure [38]. Both ImZr–SBA-15 samples with Zr/Si ratios of 0.03 and 0.1 have similar scattering features as that of bulk ZrO_2, except the second and third peaks were less intense, indicating that Zr in ImZr–SBA-15 forms ZrO_2 crystallites of smaller sizes. For the as-made Zr–SBA-15 materials of low Zr loading, only the first scattering peak was observed at 1.61 Å (uncorrected) corresponding to the nearest oxygen atoms. As the Zr loading was increased, a shoulder peak at 2.10 Å (uncorrected) grew gradually, implying that another shell of oxygen atoms with longer Zr–O bond distance was present. Morey et al. [38] reported that two different Zr–O shells, corresponding to framework Zr–O unit and surface Zr coordinated with water, are present in the Zr-incorporated MCM-48 materials. In the present study, the first oxygen shell with shorter Zr–O bond distance is probably attributed to isolated Zr species incorporated in the silica framework, and this peak is seen in all as-made samples. As to the second oxygen shell of longer Zr–O bond distance, it is probably contributed from superficial zirconia clusters coordinated to P123 copolymer or water. This proposal is supported by the TG and UV–Vis analyses, which show that the superficial zirconia clusters are not formed until the Zr/Si molar ratio is 0.03 and its amount increases with the Zr loading.

The scattering features of calcined Zr–SBA-15 samples varied in a similar trend as that of as-made ones, except the peaks were slightly broadened. Moreover, the signal/noise ratios of the scattering features were found to decrease after the samples were calcined, and even more markedly decreases were seen when the Zr loading was increased. The decrease in signal/noise ratio is due to the increase in Debye–Waller factor, which is a consequence of increase in either thermal motion or coordination chaos [39]. These results infer that although Zr species are homogeneously distributed in Zr–SBA-15, the coordinative environments of Zr become less uniform as the Zr loading increases or after the samples are calcined. On the other hand, the very weak scattering features

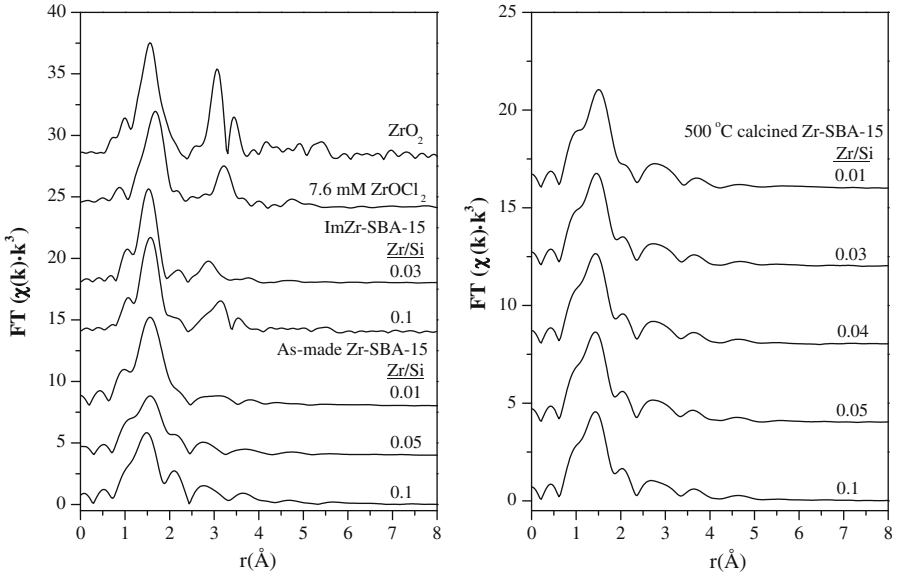

Fig. 6. Fourier transform spectra of $\chi(k) * k^3$ weighted in *R* space of as-made and calcined Zr–SBA-15 materials with various Zr/Si ratios, in comparison with the spectra of bulk ZrO_2, 7.6 mM $ZrOCl_2$ solution and ImZr–SBA-15 materials with Zr/Si ratios of 0.03 and 0.1.

at 2.5–4.0 Å (uncorrected) distance imply that the Zr species in Zr–SBA-15 are either incorporated in the framework as isolated species or on the surfaces of the mesopores as zirconia clusters, which are probably smaller than $[Zr_4(OH)_8(H_2O)_{16}]^{8+}$ tetramer.

3.1.8. NH_3-TPD

The acidities of calcined Zr–SBA-15 materials were examined by carrying out the NH_3-TPD experiment, and the profiles were compared with those of ZSM-5, HY-zeolites, Si–SBA-15 and Zr-impregnated SBA-15 materials (Fig. 7). Commercial HY-zeolite with a SiO_2/Al_2O_3 ratio of 5.3 owned largest acid amount among the studied materials. A strong and broad signal covering the temperature range of 120–450 °C was seen with the maximum at 200 °C. For ZSM-5 with a SiO_2/Al_2O_3 ratio of 230, two broad signals with medium intensities were seen at 200 and 390 °C, implying that ZSM-5 has stronger acidic strength than HY. Both the ImZr–SBA-15 and Si–SBA-15 showed almost no acidity, while the one-pot synthesized Zr–SBA-15 materials had relatively strong acidities. The desorption peaks of NH_3 on Zr–SBA-15 covered the temperature range of 130–450 °C, indicating that the acidic strength of Zr–SBA-15 is comparable to that of HY-zeolite. Moreover, the desorption peak of NH_3 grew with Zr loading, inferring the acid sites in Zr–SBA-15 are related to Zr species. However, although ImZr–SBA-15 has similar Zr loading as 0.1Zr–SBA-15, the impregnated sample has almost no acidity. These results indicate that the acidities of one-pot synthesized Zr–SBA-15 are due to isolated Zr species in the SBA-15 framework or ZrO_2 clusters on the wall surfaces rather than small ZrO_2 crystallites as those in ImZr–SBA-15 prepared by impregnated method. On the basis of NH_3-TPD peak area, the acid amounts of the studied materials decrease in the order of HY-zeolite > ZSM-5 $\geqslant$ Zr–SBA-15 > ImZr–SBA-15 $\sim$ Si–SBA-15.

3.2. Catalytic reactions

3.2.1. Pinacol rearrangement of 2,3-dimethyl-2,3-butanediol

The catalytic performances of Zr–SBA-15 materials prepared by one-pot synthesis were examined in liquid phase pinacol-type rearrangement. Fig. 8 illustrates the pinacol rearrangement over 0.1Zr–SBA-15 as a function of reaction period at 110 °C. The pinacol conversion and pinacolone yield increased linearly with the reaction period in the first 40 min. As the reaction prolonged, the reaction rate slowed down. After 2 h, pinacol was completely consumed and the yields of pinacolone and 2,3-dimethyl-2,3-butadiene (DMBD) were 81% and 19%, respectively. The pinacolone to DMBD molar ratios were kept at a constant value within 4.2–4.4 throughout the reaction period. For the purpose of comparing the activities of various catalysts, the results of the reaction after 1 h are compared hereafter.

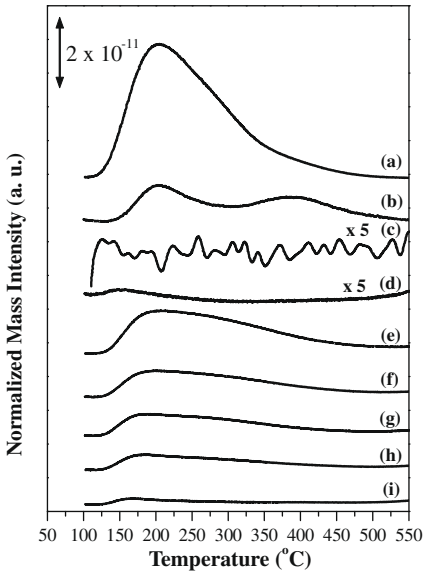

Fig. 7. NH_3-TPD profiles of (a) HY-zeolite, (b) ZSM-5, (c) ImZr–SBA-15, (d) Si–SBA-15, Zr–SBA-15 with Zr/Si ratios of (e) 0.1, (f) 0.05, (g) 0.04, (h) 0.03 and (i) 0.01, where the mass signals are collected by using $m/z = 16$.

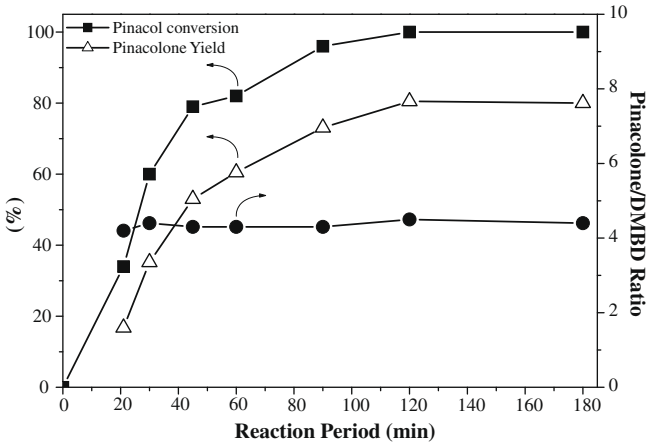

Fig. 8. Pinacol rearrangement as a function of reaction period over 0.1Zr–SBA-15 catalyst.

Table 2 summarizes the catalytic performances of various porous materials in pinacol rearrangement. Over Si–SBA-15 and ImZr–SBA-15, the pinacol conversions were very low and no pinacolone product was detected. On the other hand, one-pot synthesized Zr–SBA-15 materials were very efficient catalysts for the rearrangement reaction, and the pinacol conversion and pinacolone selectivity increased with Zr loading. Over 0.01Zr–SBA-15 with lowest Zr loading, the pinacol conversion was only 8.6%, and the pinacolone selectivity was about 61%. The values increased dramatically to 26% and 80% when the Zr/Si ratio was increased to ca. 0.03. Over 0.1Zr–SBA-15, which contains the highest Zr loading, the pinacol conversion and pinacolone selectivity reached 82% and 81%, respectively, and the pinacolone yield reached 2.7 g/g catal h. Fig. 9 correlates the pinacol conversion and acid amount in Zr–SBA-15 expressed by the relative NH_3-TPD peak area with Zr loading. The acid amount increases almost linearly with the Zr loading, while a stronger than linear increase in pinacol conversion is seen when the Zr/Si ratio is greater than 0.03. These results clearly demonstrate that the acidic sites in Zr–SBA-15 are contributed by the incorporated Zr species. Moreover, since the superficial zirconia clusters are not clearly detected until the Zr/Si ratio is higher than 0.03, the superficial zirconia clusters aggregated on the pore walls of SBA-15 are likely more accessible and efficient than the isolated Zr species in the framework in catalyzing the pinacol rearrangement reaction.

The pinacol conversions over ZSM-5 and HY-zeolites (6.0% and 15%, respectively) are lower than those over most of the Zr–SBA-15 materials, although the zeolites have larger amounts of acid sites than Zr–SBA-15. The low catalytic activities of ZSM-5 and HY-zeolites in pinacol rearrangement are probably due to the unfavorable diffusion of hydrophilic pinacol molecules into the relatively small and hydrophobic pores of zeolites. It is also noticeable that the pinacolone selectivity over HY-zeolite is similar to that over Zr–SBA-15 of ca. 80%, whereas that over ZSM-5 is only 46%. Since the pore size of ZSM-5 is the smallest among the studied materials, the pinacol rearrangement should proceed only on the outer surfaces of ZSM-5 particles. The low selectivity over ZSM-5

Table 2
Liquid phase pinacol rearrangement of 2,3-dimethyl-2,3-butandiol over various catalysts.

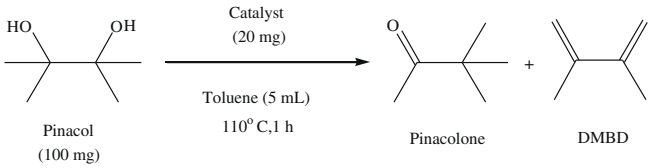

Catalyst	M/Si[a] (solid)	NH_3-TPD peak area ratio	Conversion (%)	Pinacolone	
				Yield (g/g catal h)	Selectivity (%)
None	–	–	0	0	0
Si–SBA-15	–	0.014	0.7	0	0
ZSM-5	0.0087	0.23	6.0	0.1	46
HY-zeolite	0.38	1.0	15	0.5	80
ImZr–SBA-15	0.03	n.d.[b]	0	0	0
	0.10	n.d.	0.5	0	0
Zr–SBA-15	0.017	0.024	8.6	0.2	61
	0.029	0.12	26	0.8	80
	0.044	0.17	54	1.7	79
	0.059	0.21	69	2.2	78
	0.11	0.36	82	2.7	81
Reg-Zr–SBA-15	0.11	0.36	80	2.6	82

[a] M/Si = metal to Si molar ratio.
[b] Not detectable.

indicates that the surface acid sites probably cannot stabilize the intermediate of alkyl-migration, which leads to pinacolone product, due to steric factor.

Among the catalysts examined in the present study, Zr–SBA-15 materials with Zr/Si ratios higher than 0.03 are superior to others, including ZSM-5 and HY-zeolites. Moreover, the reaction rates over Zr–SBA-15 materials are much faster than the metal-incorporated AlPO-5 materials reported previously [26]. The well-dispersed zirconia clusters containing two or more Zr centers on the wall surfaces of mesopores are likely the active sites for pinacol rearrangement.

3.2.2. Effect of solvent

The polarity of the solvent was found to have significant effect on the pinacol conversion and product selectivity. Table 3 shows the catalytic performance of 0.1Zr–SBA-15 in pinacol rearrangement using different solvents. Toluene and *o*-xylene were found to give the highest pinacol conversion and pinacolone selectivity among the solvents. The conversion and pinacolone selectivity decreased when non-polar solvents, such as *n*-decane, were used in the reaction. On the other hand, the catalytic reaction did not proceed at all in highly polar solvent, such as *n*-butanol and dimethyl sulfoxide (DMSO). The pinacol reactant is a polar compound, while the products including aldehyde, ketone and diene are relatively less polar or non-polar compounds. The mesoporous SBA-15 catalysts have hydrophilic walls, which facilitate the access of the polar reactant and also the expelling of the non-polar products from the catalytic sites. However, highly polar solvents such as butanol and DMSO probably compete with the polar reactant in adsorption on the hydrophilic walls and cover the catalytic sites up. In contrast, pinacol has low solubilities in non-polar solvents, which cannot efficiently carry the reactant to the catalytic sites for reaction. Therefore, a solvent of proper polarity is necessary for the pinacol rearrangement.

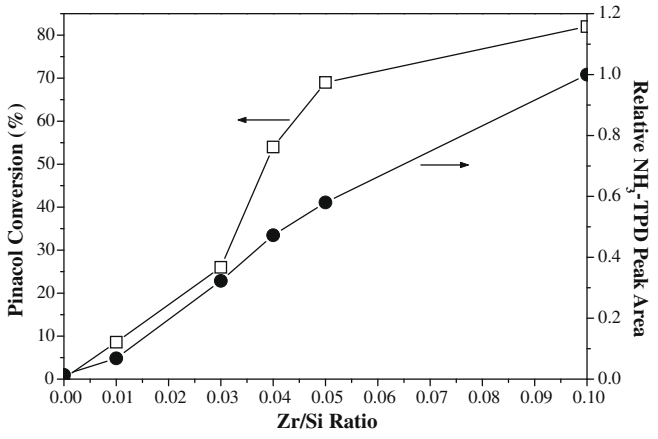

Fig. 9. Pinacol conversions and acidities of Zr–SBA-15 materials as a function of Zr contents.

3.2.3. Possible reaction mechanism

The proposed reaction mechanism of pinacol rearrangement over Zr–SBA-15 materials is illustrated in Scheme 1. On the hydrophilic surfaces of Zr–SBA-15, the OH groups of pinacol are probably coordinated onto the adjacent superficial Zr(IV) sites through oxygen atoms, while the H atoms on the hydroxyl groups may be stabilized by hydrogen bonding with lattice oxygens of the zirconia cluster to form acidic protons in the adsorbed species. In path 1,

Table 3
Pinacol rearrangement of 2,3-dimethyl-2,3-butandiol over 0.1Zr–SBA-15 in various solvents.[a]

Solvent	Dielectric constant (20 °C)	Conv. (%)	Pinacolone	
			Yield (g/g catal h)	Selectivity (%)
n-Decane	2.0	53	1.6	41
Toluene	2.2	82	2.7	81
o-Xylene	2.6	83	2.8	77
n-Butanol	18	0	0	0
DMSO	47	0	0	0

[a] Pinacol/catalyst weight ratio is 5, and the reaction is carried out at 110 °C for 1 h.

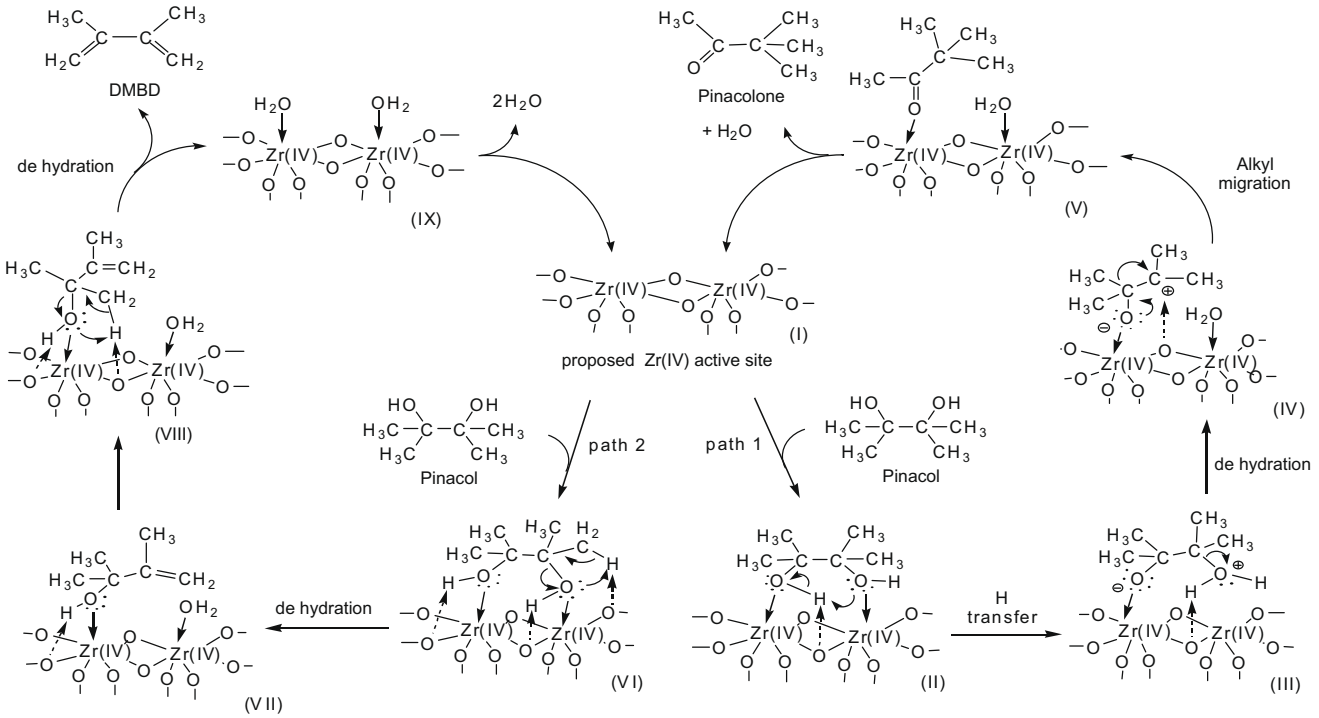

Scheme 1. Proposed reaction mechanism of pinacol rearrangement over Zr–SBA-15 materials.

the acidic proton on the OH group is ready to transfer to the other OH group on the adsorbed pinacol, resulting in intermediate (III). After dehydration, intermediate (IV) with a lattice oxygen-stabilized carbocation is formed. As the electron pair on C–O back-donates to carbon, pinacolone is formed through an alkyl-migration. On the other hand, the reaction can also go through path 2, where dehydration occurs on the surface-stabilized hydroxyl groups and the H atoms on vicinal methyl groups to generate C=C bonds. DMBD is formed by removing two molecules of water from absorbed pinacol. It is noticeable that both pinacolone and DMBD are hydrophobic molecules and can be easily expelled from the hydrophilic Zr–SBA-15 surfaces. However, it needs a solvent soluble with water to take the water product away from the superficial Zr(IV) sites, so that the catalytic active sites can be regenerated.

3.2.4. Reuse of catalyst

After the catalytic reactions, the 0.1Zr–SBA-15 catalyst was regenerated by washing with toluene several times, drying at 50 °C overnight, and then calcination at 500 °C in air for 12 h. The regenerated 0.1Zr–SBA-15 (shortly termed Reg-Zr–SBA-15) was used under the same reaction condition as that of the fresh

Table 4
Liquid phase pinacol rearrangement of (1*S*, 2*S*, 3*R*, 5*S*)-(+)-2,3-pinanediol over various catalysts.

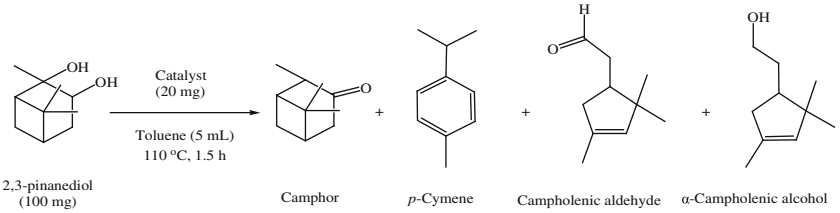

Catalyst	M/Si (solid)	Conversion (%)	Selectivity (%)			
			Camphor	p-Cymene	Aldehyde	Alcohol
None	–	0	0	0	0	0
Si–SBA-15	–	0	0	0	0	0
ZSM-5	0.0087	0	0	0	0	0
HY-zeolite	0.38	13	35	6.7	51	6.7
ImZr–SBA-15	0.10	0	0	0	0	0
Zr–SBA-15	0.017	10	35	38	24	3.3
	0.029	61	45	18	34	3.3
	0.044	76	46	16	33	4.8
	0.059	77	52	16	30	1.9
	0.11	82	50	16	32	2.1

catalyst, and the results are also listed in Table 2. The pinacol conversion and pinacolone selectivity over Reg-Zr–SBA-15 were 80% and 82%, respectively, similar to those of the first run. These results imply that the Zr–SBA-15 materials can be easily regenerated by washing and calcination and the catalytic activity is well retained in pinacol rearrangement.

3.2.5. Catalytic rearrangement of (1S, 2S, 3R, 5S)-(+)-2,3-pinanediol

The pinacol-type rearrangement of bulky (1*S*, 2*S*, 3*R*, 5*S*)-(+)-2,3-pinanediol was also examined by various catalysts used in the present study. Table 4 summarizes the results of the reaction at 110 °C for 1.5 h. Among the catalysts studied, only Zr–SBA-15 and HY-zeolite showed catalytic activities in this reaction. Moreover, Zr–SBA-15 materials with Zr/Si ratio greater than 0.03 gave much higher conversions than HY-zeolite. The pinanediol conversion was proportional to the Zr loading in the Zr–SBA-15 materials. The pinanediol conversion reached 82% in 1.5 h over 0.1Zr–SBA-15 catalyst. The main products were camphor (a product of H-migration), p-cymene (a product in combination of alkyl- and H-migration) and campholenic aldehyde (a product of alkyl-migration). In addition, a small amount of α-campholenic alcohol was found, probably through the reduction of campholenic aldehyde by solvent. The H-migration product became favorable to the alkyl-migration ones over Zr–SBA-15 materials with Zr/Si ratio greater than 0.03, and it is in consistent with that observed in liquid phase acid-catalyzed reaction [27,40]. These results imply that diffusion of the large reactant and product molecules in the mesopores of Zr–SBA-15 is apparently not hampered. In contrast, the alkyl-migration products are favorable to H-migration camphor over HY-zeolite, implying the diffusion of bulky pinanediol into the zeolitic pores is restricted.

4. Conclusions

Well-ordered SBA-15 mesoporous materials with high loadings of Zr(IV) have been successfully synthesized by one-pot co-condensation in a self-generated acidic environment with the aid of NaCl. The resultant Zr–SBA-15 materials contain high surface area, large pore volume and narrow PSD. Zr(IV) is incorporated in the silica frameworks as isolated Zr species when the Zr/Si ratio is lower than 0.03, and it aggregates and forms small zirconia clusters containing two or more Zr centers on the wall surfaces of SBA-15 when Zr loading is increased or after the samples are calcined. The NH_3-TPD analysis showed that the acid amounts of Zr–SBA-15 materials were proportional to the Zr loading and the acidic strength was comparable to that of HY-zeolite. The acid amounts of the studied materials decrease in the order of HY > ZSM-5 ⩾ Zr–SBA-15 > ImZr–SBA-15 ∼ Si–SBA-15. When used as the catalysts in liquid phase pinacol-type rearrangement reactions, Zr–SBA-15 synthesized by one-pot co-condensation showed much higher catalytic activities than others. The superficial zirconia clusters aggregated on the pore walls of SBA-15 are more accessible and efficient than the isolated Zr species in the framework in catalyzing the pinacol rearrangement reaction. In contrast, ImZr–SBA-15 which contains small ZrO_2 crystallites has no acid sites based on NH_3-TPD, and it shows no catalytic activity in pinacol rearrangement. In pinacol rearrangement, the catalytic activities decreased in the order of Zr–SBA-15 > HY-zeolite > ZSM-5 > Si–SBA-15 ∼ ImZr–SBA-15. The relatively low activities of microporous HY and ZSM-5 zeolites are probably due to the diffusion limitation of hydrophilic pinacol molecules into the small and hydrophobic zeolitic pores. By using 0.1Zr–SBA-15 as the catalyst, the pinacolone yield of 2.7 g/g catal h and selectivity of 81% could be reached in 1 h at 110 °C. The used Zr–SBA-15 catalysts were easily regenerated by washing and calcination, and the high activities in pinacol rearrangement were retained. Moreover, the large mesopores of Zr–SBA-15 materials also facilitated the pinacol-type rearrangement of bulky (1*S*, 2*S*, 3*R*, 5*S*)-(+)-2,3-pinanediol. The major product over Zr–SBA-15 was camphor, a product of H-migration.

Acknowledgments

The financial supports from the National Science Council and the Ministry of Education, Taiwan, are gratefully acknowledged. Acknowledgments are also extended to Chih-Yuan Tang and Ching-Yen Lin of Instrumentation Center, National Taiwan University, Taiwan, for TEM and SEM experiments, and Chin-Nan Ke of National Tsing-Hua University, Taiwan, for the ICP-AES experiment.

References

[1] X. Fang, G.E. Frywell, L.Q. Wang, A.Y. Kim, J. Liu, K.M. Kemner, Science 276 (1997) 923.
[2] J.M. Sun, H. Zhang, R.J. Tian, D. Ma, X.H. Bao, D.S. Su, H.F. Zou, Chem. Commun. (2006) 1322.
[3] A. Corma, Chem. Rev. 97 (1997) 237.
[4] X. Wang, C.C. Chen, S.Y. Chen, Y. Mou, S. Cheng, Appl. Catal. A 281 (2005) 47.
[5] Y. Wang, C.M. Yang, W. Schmidt, B. Spliethoff, E. Bill, F. Schüth, Adv. Mater. 17 (2005) 53.
[6] H. Yang, D.Y. Zhao, J. Mater. Chem. 15 (2005) 1217.
[7] S. Baskaran, J. Liu, K. Domansky, N. Kohler, X. Li, C. Coyle, G.E. Frywell, S. Thevuthasan, R.E. Williford, Adv. Mater. 12 (2000) 291.
[8] C.M. Yang, A.T. Cho, F.M. Pan, T.G. Tsai, K.J. Chao, Adv. Mater. 13 (2001) 1099.
[9] M.H. Bartl, S.P. Puls, J. Tang, H.C. Lichtenegger, G.D. Stucky, Angew. Chem. Int. Ed. 43 (2004) 3037.
[10] D. Zhao, J. Feng, Q. Huo, N. Melosh, G.H. Fredrickson, B.F. Chmelka, G.D. Stucky, Science 179 (1998) 548.
[11] J.S. Beck, J.C. Vartuli, W.J. Roth, M.E. Leonowicz, C.T. Kresge, K.D. Schmitt, C.T.W. Chu, D.H. Olson, E.W. Sheppard, S.B. McCullen, J.B. Higgins, J.L. Schlenker, J. Am. Chem. Soc. 114 (1992) 10834.
[12] J.A. Melero, G.D. Stucky, R.V. Grieken, G. Morales, J. Mater. Chem. 12 (2002) 1664.
[13] S.Y. Chen, C.Y. Tang, W.T. Chuang, J.J. Lee, Y.L. Tsai, J.C.C. Chan, C.Y. Lin, Y.C. Liu, S. Cheng, Chem. Mater. 20 (2008) 3906.
[14] S.Y. Chen, L.Y. Jang, S. Cheng, Chem. Mater. 16 (2004) 4174.
[15] B.L. Newalkar, J. Olanrewaju, S. Komarneni, J. Phys. Chem. B 105 (2001) 8356.
[16] C. Ngamcharussrivichai, P. Wu, T. Tatsuimi, J. Catal. 227 (2004) 448.
[17] P. Wu, T. Tatsumi, K. Komatsu, T. Yashima, Chem. Mater. 14 (2002) 1657.
[18] B.L. Newalker, J. Clanrewaju, S. Komarneni, Chem. Mater. 13 (2001) 552.
[19] A. Vinu, D.P. Sawant, K. Ariga, K.Z. Hossain, S.B. Halligudi, M. Hartmann, M. Nomura, Chem. Mater. 17 (2005) 5339.
[20] S.Y. Chen, H.D. Tsai, W.T. Chuang, J.J. Lee, C.T. Tang, C.Y. Lin, S. Cheng, J. Phys. Chem. C 113 (2009) 15226.
[21] C.W. Chiang, A. Wang, B.Z. Wan, C.Y. Mou, J. Phys. Chem. B 109 (2005) 18042.
[22] H. Song, R.M. Rioux, J.D. Hoefelmeyer, R. Komor, K. Niesz, M. Grass, P. Yang, G.A. Somorjai, J. Am. Chem. Soc. 128 (2006) 3027.
[23] C.J. Collins, J. Am. Chem. Soc. 77 (1955) 5517.
[24] W.E. Bachmann, Org. Synth. 2 (1943) 71.
[25] E.J. Corey, R.L. Danheier, S. Chandrasekaran, J. Org. Chem. 41 (1976) 260.
[26] B.-Y. Hsu, S. Cheng, Micropor. Mesopor. Mater. 21 (1998) 505.
[27] M. Hsien, H.-T. Sheu, T. Lee, S. Cheng, J.-F. Lee, J. Mol. Catal. A 181 (2002) 189.
[28] R. Ganguly, V.K. Aswal, P.A. Hassan, I.K. Gopalakrishnan, J.V. Yakhmi, J. Phys. Chem. B 109 (2005) 5653.
[29] C. Yu, B. Tian, J. Fan, G.D. Stucky, D. Zhao, J. Am. Chem. Soc. 124 (2002) 4556.
[30] W. Guo, J.-Y. Park, M.-O. Oh, H.-W. Jeong, W.-J. Cho, I. Kim, C.-S. Ha, Chem. Mater. 15 (2003) 2295.
[31] Y.Q. Wang, C.M. Yang, B. Zibrowius, B. Spliethoff, M. Linden, F. Schuth, Chem. Mater. 15 (2003) 5029.
[32] D. Das, C.-M. Tsai, S. Cheng, Chem. Commun. (1999) 473.
[33] S.Y. Chen, S. Cheng, Chem. Mater. 19 (2007) 3041.
[34] C.K. Krishnan, T. Hayashi, M. Ogura, Adv. Mater. 20 (2008) 2131.
[35] A. Emeline, G.V. Kataeva, A.S. Litke, A.V. Rudakova, V.K. Ryabchuk, N. Serpone, Langmuir 14 (1998) 5011.
[36] A. Clearfield, P.A. Vaughan, Acta Cryst. 9 (1956) 555.
[37] S.Y. Chen, L.Y. Jang, S. Cheng, J. Phys. Chem. B 110 (2006) 11761.
[38] M.S. Morey, G.D. Stucky, S. Schwarz, M. Froba, J. Phys. Chem. B 103 (1999) 2037.
[39] E. Bus, J.T. Miller, A.J. Kropf, R. Prins, J.A. van Bokhoven, Phys. Chem. Chem. Phys. 8 (2006) 3248.
[40] K. Nakamura, Y. Osamura, J. Am. Chem. Soc. 115 (1993) 9112.